Heliyon 10 (2024) e35284

Contents lists available at ScienceDirect

Heliyon

journal homepage: www.cell.com/heliyon

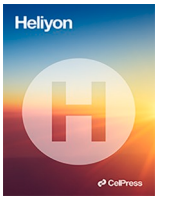

Research article

Biosynthesized and chemically synthesized Ag/TiO_2 nanocomposites: Effect of reaction parameters on synthesis using watermelon rind extract and comparative analysis

Marylyn Mugure Gathiru [a,*], Emilly Obuya [b], Naumih M. Noah [c], Erick Masika [a]

[a] Department of Chemistry, Kenyatta University, P.O. Box 43844-00100 Nairobi, Kenya
[b] Department of Chemistry, Russell Sage College, P.O. Box 65 1st Street Troy, NY, 12180, United States
[c] School of Pharmacy and Health Sciences, United States International University-Africa, P.O. Box 14634-00800, Nairobi, Kenya

ARTICLE INFO

Keywords:
Modification
Watermelon rind extract (WMRE)
Silver/ titania (Ag/TiO_2)

ABSTRACT

This work synthesized Ag/TiO_2 nanocomposite via an aqueous reduction method using a green and chemical reducing agent. *Citrullus lanatus* (watermelon) rind extract (WMRE) and sodium borohydride ($NaBH_4$) were used as the reducing agents during green synthesis and chemical synthesis, respectively. During green synthesis, a pH of 12, a reaction time of 45 min, and an operating temperature of 100 °C yielded the best visible light activity. The biosynthesized and chemically-synthesized Ag/TiO_2 were compared using UV–Vis spectroscopy, X-ray fluorescence spectroscopy (XRF), X-ray diffraction spectroscopy (XRD), Fourier transform infrared spectroscopy (FTIR), energy dispersive spectroscopy-scanning electron microscopy (EDS-SEM) and transmission electron microscopy (TEM). Synthesis using WMRE yielded spherical Ag nanoparticles modified on the surface of TiO_2 nanoparticles. The Ag nanoparticles had enhanced monodispersity with an average diameter of 7.48 ± 4.06 nm. Therefore, the developed WMRE green synthesis method provides a simple, less chemical-intensive, and effective alternative to chemical synthesis.

1. Background

Green synthesis is crucial for modern nanotechnology development. It involves using plant extracts that are environmentally safe, low-cost, and renewable feedstock, enhancing safety for the environment and humans [1]. A considerable amount of waste is generated from consuming fruits with seeds and peels perceived as inedible. This waste contributes to an increase in green waste, necessitating the study of their composition and physicochemical properties to guide applications in green engineering and chemical technologies [2]. These environmentally friendly applications have gathered interest since there is an endless list of possible peels and seeds. The *Citrullus lanatus* (watermelon) rind is generally discarded due to its bitter taste. To reduce the generation of green waste, it has been used in the production of candy, fruit butter, biscuits, cake mayonnaise, bread, and in the synthesis of nanoparticles [3,4].

The use of watermelon rind extract (WMRE) in green synthesis is attributed to its phenolic acid components. These phenolic acids, such as chlorogenic acid, sinapic acid, vanillic acid, caffeic acid, myricetin, and gallic acid [5], have been employed in producing various nanoparticles. Studies by Ndikau et al. [6] and Sackey et al. [7] focused on the use of chlorogenic acid, and gallic, L-glutamic,

* Corresponding author.
E-mail address: gathirumarylyn@gmail.com (M.M. Gathiru).

https://doi.org/10.1016/j.heliyon.2024.e35284
Received 5 February 2024; Received in revised form 24 July 2024; Accepted 25 July 2024
Available online 26 July 2024

and sinapic acids as the reducing agents in *Citrullus lanatus* rind extract and *Phoenix dactylifera* for the synthesis of Ag and manganese oxide (Mn_3O_4) nanoparticles. They observed a decrease in the concentration of these acids, which was attributed to their reducing and stabilizing activity. As the presence of phenolic compounds forms the basis of green synthesis, this field offers ample opportunities for exploration using different plants and plant parts.

The use of Ag nanoparticles in metal-enhanced photocatalysis has attracted significant attention [8]. Photocatalysis is the acceleration of a photoreaction using photocatalysts like TiO_2. TiO_2 is the most utilized photocatalyst due to its lower toxicity and dependence on pH and higher resistance to photocorrosion [9], with applications majorly in environmental remediation [10] and antimicrobial disinfection [9]. Though highly effective, applications are limited by its high recombination rate and inability to utilize visible light radiation. Metal-enhanced photocatalysis is one of the explored solutions to improve TiO_2 photocatalytic activity [11].

Metal-enhanced photocatalysis involves incorporating metal impurities into the photocatalyst to reduce the recombination rate [12]. These impurities are added either into the TiO_2 crystalline structure or modified onto the surface [8]. Since chemical reactions occur on the TiO_2 surface, surface modification offers a more straightforward solution for improved photocatalysis [13]. Essentially, metal surface modification results in a Schottky barrier, which acts as an electron trap, slowing down the rate of electron recombination [14]. Additionally, the use of noble metals yields visible light activity due to their surface plasmon resonance (SPR) [11].

The modification of the TiO_2 surface with Ag nanoparticles involves their reduction on the surface. Synthesis of Ag nanoparticles can be achieved using chemical, green, and physical methods. The effectiveness of these methods is shown in Table 1. Green synthesis of Ag/TiO_2 nanocomposite has been done using *Padina tetrastromatica* (seaweed) extract [15], *Eucalyptus globulus* L. extract [16], *Mirabilis jalapa* plant extract [17], and grape cake [18]. Skiba et al. [18] compared the plasma-liquid synthesis of Ag/TiO_2 nanocomposites using different capping agents. They found that higher antimicrobial activity was achieved when a green capping agent (grape cake) was used, pointing to the effectiveness of green synthesis.

Little attention has been given to the use of green waste components during synthesis based on the reported Ag/TiO_2 green synthesis methods. This study, therefore, synthesized Ag/TiO_2 nanocomposite using WMRE while evaluating the effect of various reaction parameters. It also compared the efficiency of green and chemical synthesis methods for Ag/TiO_2.

2. Materials and methods

2.1. Preparation of WMRE

WMRE preparation was done following the Ndikau et al. [6] method. One Charleston grey variety ripe watermelon was washed with deionized water (DI). It was then cut into four equal portions, followed by removing the red pulp to obtain the rind. Subsequently, the rind was cut into 10 mm-by-10mm sizes, weighed at 150 g, and placed in a beaker (1000 mL). Consequently, 500 mL of DI was added and the mixture was blended for 10 min. The resulting solution was poured back into the beaker, magnetically stirred at 100 °C for 10 min, and cooled at room temperature. The final step involved filtration using Whatman no. 1 filter paper into a flask, giving the WMRE, which was stored at 4 °C.

2.2. Green synthesis of Ag/TiO_2 nanocomposite using WMRE

Initially, 0.2 g TiO_2 nanoparticle powder was dissolved in 100 mL DI using ultrasonic treatment for 10 min. This was followed by adding 0.02 g of $AgNO_3$, pH adjustment to 7 by adding 1 % HNO_3 drops, and 30 min of magnetic stirring. After this, 30 mL WMRE was added, followed by pH adjustment to 12 using 33 % NH_4OH and magnetic stirring at 100 °C for 45 min. The resulting solution was then centrifuged, followed by washing; this was done thrice. To obtain the nanocomposite powder, freeze-drying was done. The resulting powder was stored in sealed polyethylene terephthalate (PET) Petri dishes labeled WMAT and kept at room temperature until further use.

2.3. Evaluation of the effect of operating conditions for green synthesis

Time, temperature, and pH were selected as the operating conditions whose effect was to be investigated during the synthesis of Ag/TiO_2 nanocomposite using WMRE. These conditions were chosen due to their proven impact on nanoparticle shape, size, and size homogeneity.

First, the reaction was conducted at 15, 25, 35, 45, and 60 min, as well as at 24 and 48 h while maintaining a constant pH of 12 and temperature of 100 °C. The resulting solutions were centrifuged, washed thrice, and characterized using UV–Vis spectroscopy.

This was followed by varying the reaction temperature to 25, 40, 80, and 100 °C while keeping the time and pH fixed at 45 min and

Table 1
Comparison of the effectiveness of different Ag nanoparticles synthesis methods.

Synthesis method	Reducing agent	Nanoparticle size	Morphology	Ref
Plasma discharge		36.50 nm	Spherical	[19]
Chemical synthesis	Hydrazine hydrate and sodium citrate	24.00 nm	Spherical	[20]
Green Synthesis	*Prunus persica* L.	10–20.00 nm	Spherical	[21]
Green Synthesis	*Citrullus lanatus* (watermelon) rind extract (WMRE)	7.48 ± 4.06 nm	Spherical	

12, respectively. Subsequently, centrifugation and characterization using UV–Vis spectroscopy were conducted.

The pH was adjusted to 8, 10, and 12 while keeping other reaction parameters constant at 45 min and 100 °C. This pH variation was performed after adding the WMRE. The nanocomposites obtained from centrifugation were characterized using UV–Vis spectroscopy.

2.4. Chemical synthesis of Ag/TiO_2 nanocomposite using sodium borohydride

Chemical synthesis was done following the Niño-Martínez et al. [22] method, which is briefly described. At the start, a solution of TiO_2 nanoparticles and $AgNO_3$ was prepared at a molar ratio of 1:25. Sodium borohydride ($NaBH_4$) (0.1 mmol) was added, accompanied by a pH adjustment to 10 followed by 35 min of magnetic stirring. The resultant solution was centrifuged and calcined to obtain the Ag/TiO_2 powder, which was stored in sealed PET Petri dishes labeled NBAT at room temperature.

2.5. Characterization

The visible light activity of TiO_2, WMAT, and NBAT was evaluated using the SHIMADZU UV–Vis Spectrophotometer UV-1900. SHIMADZU IR –Spirit with QATR-S Fourier transform IR spectrophotometer was used to investigate the functional groups in TiO_2, WMAT, and NBAT. The elemental composition of the TiO_2, WMAT, and NBAT was obtained using RUKER XRF S1 TITAN/TRACER 5/CTX. X-ray powder crystallization analysis of the TiO_2, WMAT, and NBAT was accomplished via a Thermo Scientific™ ARL™ EQUINOX 100 X-ray Diffractometer equipped with Cu Kα1 ($\lambda = 1.5406$ Å). Surface micrographs were obtained using a FEI XL40 ESEM equipped with two EDAX Sapphire Si(Li) EDS detectors with up-to-date MLA software. TiO_2 and Ag nanoparticle morphology were analyzed using Oxford SDD Detector for TEM: X-MaxN 80T.

3. Results and discussion

Utilizing WMRE during the synthesis of $AgTiO_2$ ensures non-hazardous synthesis while achieving both reduction and stabilization of the nanoparticles. This green synthesis process is shown in Fig. 1 which details the possible reactions during synthesis and the TEM image of the synthesized nanocomposite. Chlorogenic acid, caffeic acid, and gallic acid, contained in WMRE, have been shown to effectively reduce nanoparticles during green synthesis, indicating their potential to reduce and stabilize Ag nanoparticles on the TiO_2 surface [23,24].

3.1. Green synthesis of Ag/TiO_2 using WMRE

Extraction of phenolic acids from the watermelon rind was performed using DI due to its high purity, low cost compared to other solvents, and contribution to the universal goal of reducing the use of harsh chemicals [25]. Ho et al. [26] found that a high total phenolic content was achieved when water was used as the extracting agent for watermelon rind powder. They attributed this to the interaction between the hydrogen polar sites in the extract and the solvent. These findings justified using DI water as the extracting solvent in this work.

The UV–Vis spectra obtained during the variation of the operating time, temperature, and pH conditions are shown in Fig. 2.

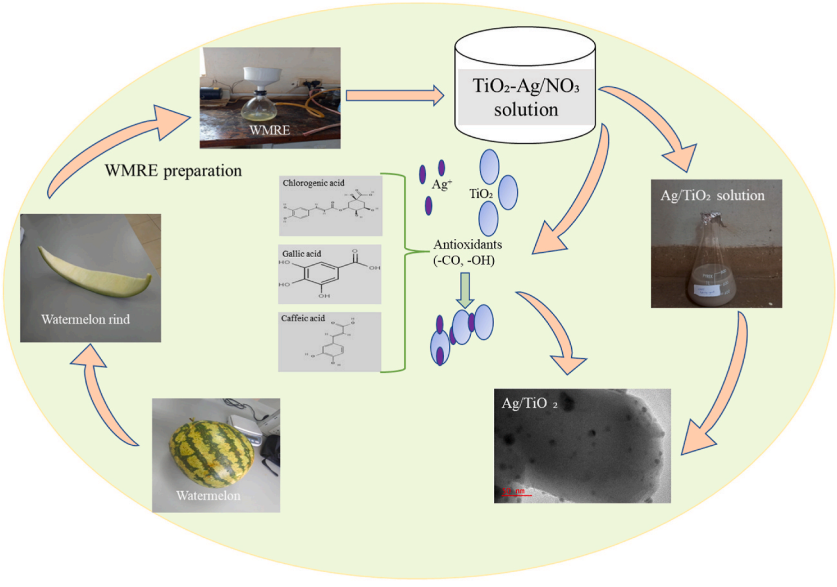

Fig. 1. Overall schematic representation for the green synthesis of Ag/TiO_2 using WMRE and a TEM image of Ag/TiO_2 nanocomposite.

Specifically, increasing reaction time favored WMAT synthesis, which gave the best peak in the visible light region. The absence of peaks in the visible light region at 15 and 25 min indicated that this time was insufficient for forming and modifying Ag nanoparticles. Visible light activity was observed at 35, 45, and 60 min and also at 24 and 48 h. A higher absorbance with a narrower peak was observed at 440 nm after 45 min of reaction, indicating the formation of smaller nanoparticles. Synthesis beyond this time shifted the absorbance to a longer visible light wavelength (500 nm) with a broader peak, as the synthesis time increased from 60 min to 48 h. The longer wavelength of these peaks indicated an increase in nanoparticle size and agreed with the findings of Wang and Cao [27] who found that the red shift in UV–Vis absorbance of Ag nanoparticles was directly correlated with an increase in nanoparticle size. Therefore, 45 min was chosen as the optimal reaction time. Similarly, Vasyliev et al. [2] found that the synthesis of Ag nanoparticles using pomegranate peel extract, grape pomace extract, and hot water as the extracting solvent reduced the reaction time. Beyond the optimal time, the high number of WMRE active sites resulted in the fast formation of small nanoparticles, which then agglomerated [27].

The temperature was varied at different levels: room temperature (25 °C), 40 °C, 80 °C, and 100 °C to assess its impact on WMAT synthesis. The results indicated that an increase in temperature promoted WMAT synthesis. Mainly, visible light activity was only observed at 80 and 100 °C (Fig. 2). A higher temperature, 100 °C, was found to result in the highest peak in the visible light region, indicating the formation of smaller Ag nanoparticles, which in turn yielded better activity in this region [28]. Kobese [29] found that an increase in temperature favored the synthesis of Ag/TiO_2 using tea extract from *Aspalathus linearis*. They attributed this to the temperature increase promoting nucleation over the growth of nanoparticles.

Similarly, a higher pH enhanced WMAT synthesis (Fig. 2). Specifically, visible light activity was only detected at pH 10 and 12. However, the peak with the highest absorbance in the visible light radiation region, indicating the formation of smaller nanoparticles, was at a pH of 12. Amin et al. [30] also found that high pH promotes the formation of small and highly dispersed Ag nanoparticles during synthesis using *Solanum xanthocarpum* berry extract. This is attributed to the high pH, which increases the number of active sites in plant extracts, effectively reducing and stabilizing the Ag nanoparticles.

3.2. UV–Vis spectroscopy

The visible light activity of WMAT and NBAT was compared to assess the effectiveness of the green and chemical synthesis methods. Absorbance peaks were observed in the visible light region at 420 nm (absorbance; 0.36 a.u) and 440 nm (absorbance; 0.018 a.u) for WMAT and NBAT, as seen in Fig. 2, with an insert showing the visible light peaks for NBAT. These peaks indicated the successful modification of TiO_2 with Ag nanoparticles, which agrees with Niño-Martínez et al. [22] and Purnomo et al. [17] who synthesized Ag/TiO_2 using $NaBH_4$ and *Mirabilis jalapa* plant extract as the reducing agents, respectively, and detected visible light

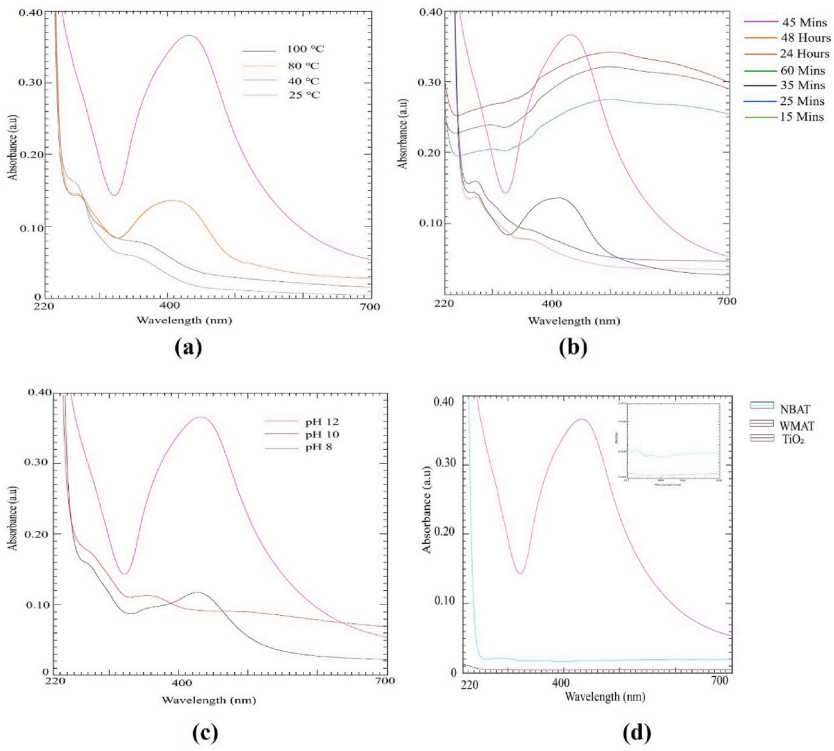

Fig. 2. UV–Vis spectra showing the effect of temperature (a), time (b), and pH (c) on the synthesis of Ag/TiO_2 nanocomposite using WMRE (WMAT), and the UV–Vis spectra for WMAT and NBAT with an insert showing the visible light peak for NBAT (d).

activity with absorbance peaks at 450 nm. Even though visible light activity was achieved using chemical and green synthesis methods, the absorption peak for the latter had a higher absorbance (indicating better visible light activity).

3.3. FTIR analysis

FTIR analysis was done to identify the functional groups in the TiO_2 nanoparticles and synthesized nanocomposites. The drying step used to obtain the nanocomposite powders differed between the two synthesis methods. WMAT was dried following a freeze-drying method, whereas NBAT was dried via calcination. Freeze-drying was conducted for WMAT to retain the active capping agents in the WMRE biomass for FTIR characterization. Even though freeze-drying enhances nanoparticle size distribution and prevents agglomeration, agglomeration was still observed in this work, as shown in Fig. 7.

Fig. 3 shows the FTIR spectra of TiO_2, WMAT, and NBAT. The absorption bands for TiO_2 and WMAT observed at 3338 and 3308 cm^{-1}, respectively, were attributed to –OH bending vibration [31]. The bands observed at 2974 and 2977 cm^{-1} in the TiO_2 nanoparticles and synthesized nanocomposites were attributed to C–H stretching vibrations, while those at 1068 cm^{-1} were attributed to C–O stretching vibration [32]. The peak characteristic of Ti–O–Ti stretching at 1465 cm^{-1} shifted to 1383 cm^{-1} after modification with Ag nanoparticles [33]. Moreover, the bands at 470 cm^{-1} were attributed to the oxide structure of TiO_2 [30]. Notably, a peak unique to WMAT was observed at 1649 cm^{-1} and ascribed to C=O bond stretching vibration [34]. The C=O bond originated from the WMRE biomass in the synthesized nanocomposite.

The identified functional groups present in WMAT and absent in NBAT were used to compare the two synthesis methods. Green synthesis of nanoparticles involves two significant steps: reduction of the precursor metal ion and its stabilization. The steps for Ag/TiO_2 synthesis using chlorogenic acid, contained in WMRE, are detailed in Fig. 4. Plant extracts contain polyphenols with hydroxyl and carbonyl groups in their aromatic rings, which reduce and stabilize nanoparticles. During the first step, the polyphenol undergoes oxidation, forming an anion of the polyphenol and reducing the Ag^+. The reduction potential of Ag^+/Ag^0 is 0.8, while that of the plant polyphenols ranges between 0.3 and 0.8 V, giving a positive ΔE, and points to the reaction occurring spontaneously [35,36]. The second step, stabilization, involves chelation, where the polyphenol anion surrounds the Ag. Mallikarjuna et al. [37] used *Ocimum sanctum* leaf extract to synthesize Ag nanoparticles and observed that the nanoparticles had a thin protein layer composed of a C=O functional group. The presence of the C=O functional group in WMAT supported these findings. Chemical synthesis, done following the Niño-Martínez et al. [22] method, utilized $NaBH_4$, which only acts as a reducing agent and not a capping agent [38]; an absorption peak for the C=O was therefore absent [39]. Green synthesis involves a single reducing and capping agent, making it a straightforward synthesis method compared to chemical methods, which require separate reducing and capping agents.

3.4. Elemental analysis

Elemental analysis was conducted using XRF and EDS spectroscopy. The composition of the major elements in pure TiO_2, WMAT, and NBAT are shown in Table 2. In this study, the green and chemical synthesis methods resulted in 10.3966 % modification and 17.8652 % modification, respectively.

During EDS analysis (Fig. 5), elemental carbon (C) was identified in the TiO_2 nanoparticles and synthesized nanocomposites. The chemical synthesis method resulted in a decrease in the carbon content since the modified Ag nanoparticles displaced it. Even though this displacement was also true for WMAT, an increase in the carbon content was observed. This increase is accredited to the stabilization effects of the C=O groups retained in the nanocomposite from the WMRE biomass. Elemental chlorine (Cl) was also detected during green synthesis due to the presence of a chlorine polyphenol complex in WMRE, 9-(2′2′-Dimethylpropanoilhydrazono)-3,6-dichloro-2,7-bis[2-(diethylamino)-ethoxy]fluorine [40]. Furthermore, elemental Al was only observed in EDS, not in XRF, and was attributed to a coating of Al_2O_3 on TiO_2 nanoparticles. The absence of Al in XRF could be attributed to the detection limit's dependence

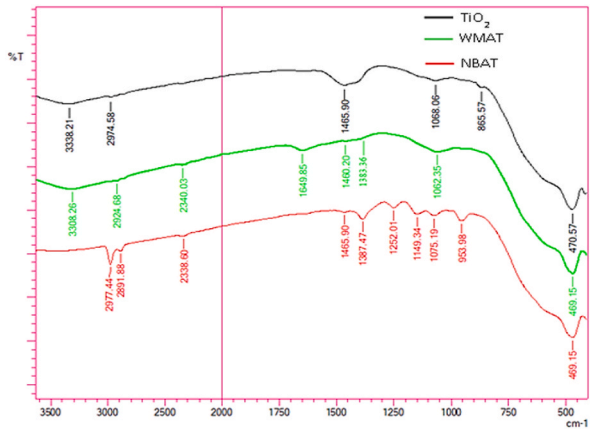

Fig. 3. FTIR spectra of the TiO_2 nanoparticles and synthesized nanocomposites.

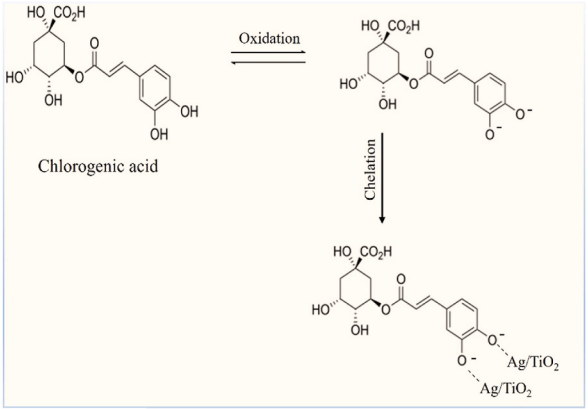

Fig. 4. Possible mechanism of Ag/TiO_2 synthesis using chlorogenic acid in WMRE.

Table 2
Percentage weight elemental composition of the TiO_2 nanoparticles and synthesized nanocomposites obtained from XRF analysis.

Element wt%	Ti	Mg	Si	Zn	Ag
TiO_2	95.56	0.40	0.48	1.60	–
WMAT	85.46	–	0.28	1.78	10.40
NBAT	77.94	–	0.31	1.88	17.87

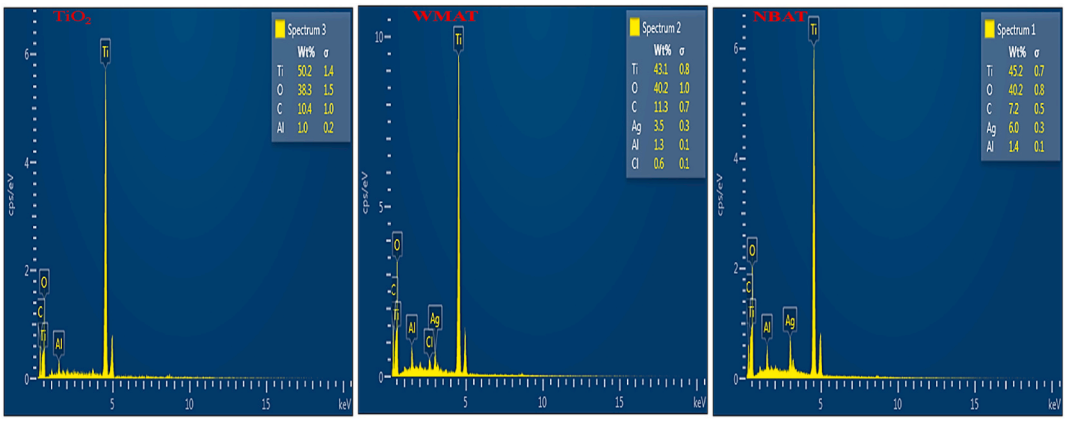

Fig. 5. EDS elemental composition of the TiO_2 nanoparticles and synthesized nanocomposites.

on counting time, element mass, and sample composition [41]. These factors may have compromised the detection of Al in TiO_2, NBAT, and WMAT.

3.5. XRD studies

XRD analysis was used to perform the phase identification and crystallite size determination of the TiO_2 nanoparticles and nanocomposites. The X-ray diffraction spectra for TiO_2, WMAT, and NBAT are shown in Fig. 6. Diffraction peaks for TiO_2 nanoparticles in the tetragonal rutile phase were detected at two-theta (2θ) = 28.00°, 31.28°, 33.61°, 34.67°, 36.24°, 46.81°, 54.77° and 65.85°, matching the (110), (110), (110), (101), (101), (210), (211) and (221) crystal planes, respectively [ICSD No. 00-021-1276]. The peak splitting observed in the (110) and (101) crystal planes was attributed to various stresses [42]. Meanwhile, peaks for the tetragonal anatase phase were detected at two-theta (2θ) = 37.78°, 45.93° and 66.93°, matching the (004), (200) and (116) crystal planes, respectively [ICSD No. 00-021-1272]. In both WMAT and NBAT there were major diffraction peaks detected at two-theta (2θ) = 26.09° and 34.53°, matching the rutile (110) and (101) crystal planes respectively [ICSD No. 00-021-1276] and two-theta (2θ) = 52.49°, matching to the anatase (105) crystal plane [ICSD No. 00-021-1272].

Similar significant peaks were observed in the synthesized nanocomposites and TiO_2 nanoparticles but with different intensities. This indicates that no new peaks were formed. Habibi and Nasr-Esfahani [43] suggested that this was due to the uniform distribution of

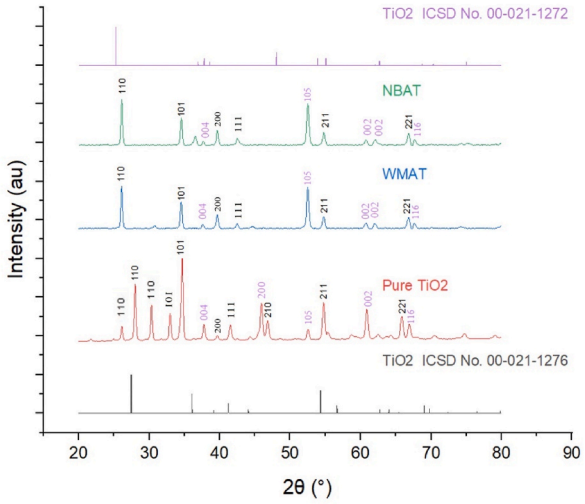

Fig. 6. X-ray diffraction spectra of TiO_2 nanoparticles and synthesized nanocomposites, showing the ICSD No. 00-021-1272 and ICSD No. 00-021-1276 TiO_2 card numbers.

the Ag nanoparticles. Furthermore, the concentration of the modified Ag nanoparticles was low, possibly lower than the diffractometer's detection limit, as suggested by Mosquera et al. [44].

The crystallite sizes of TiO_2, WMAT, and NBAT were calculated using the Debye-Scherrer formula detailed in Equation (3.1) and found to be 28.34 nm, 26.73 nm, and 26.64 nm for TiO_2 nanoparticles, WMAT, and NBAT, respectively. This finding indicates that modification with Ag generally inhibits grain growth. More specifically, a slight decrease in the anatase crystallite size from 25.07 nm in TiO_2 to 23.91 nm and 23.08 nm for WMAT and NBAT, respectively, and a slight increase in rutile crystallite size from 28.86 nm in TiO_2 to 30.54 nm and 30.47 nm for WMAT and NBAT respectively were observed.

This was attributed to the inhibition of grain growth for the anatase phase and an acceleration of grain growth for the rutile phase due to the effect of the modified Ag nanoparticles [45]. Comparing the green and chemical synthesis methods in this analysis revealed that they yielded similar grain growth inhibition and acceleration effects for the anatase and rutile phases, respectively.

$$D = \frac{K\lambda}{\beta \, Cos \, \theta} \qquad \text{Equation 3.1}$$

The percentage phase composition for the rutile and anatase phases in the TiO_2 nanoparticles, NBAT, and WMAT were calculated using Equation (3.2) [46] and are detailed in Table 3.

$$w_R = \frac{I_R}{0.884 I_A + I_R} \qquad \text{Equation 3.2}$$

3.6. Morphology of the synthesized nanocomposite powders

The morphology of the TiO_2 nanoparticles, WMAT, and NBAT was assessed using SEM. The micrographs obtained are shown in Fig. 7 and include the 2kx, 4kx, and 6kx magnifications. When TiO_2 was modified with Ag, the surface texture changed, leading to an increase in roughness. This change in surface roughness was directly correlated with the amount of modified Ag nanoparticles. As a result, NBAT was discovered to have greater roughness than WMAT.

The synthesized WMAT and NBAT had different morphologies. In the NBAT, the Ag nanoparticles were tightly packed and evenly distributed on the surface of the TiO_2 nanoparticles. In contrast, the Ag nanoparticles in the WMAT formed agglomerates on the surface of TiO_2. This agglomeration resulted from the electrostatic attraction of the layer of WMRE stabilizing agents on the Ag nanoparticles' surface. Similarly, Aminuzzaman et al. [47] synthesized partially agglomerated zinc oxide (ZnO) nanoparticles using *Garcinia mangostana* fruit pericarp aqueous extract. They attributed agglomeration to the electrostatic attraction of the layer of biomass on the surface of the nanoparticles. According to these findings, comparing chemical and green synthesis shows that chemical synthesis is

Table 3
Weight fraction of rutile and anatase phases in TiO_2 nanoparticles, WMAT, and NBAT.

Sample	Rutile fraction (%)	Anatase fraction (%)
TiO_2	61.72	38.28
WMAT	53.08	46.92
NBAT	53.08	46.92

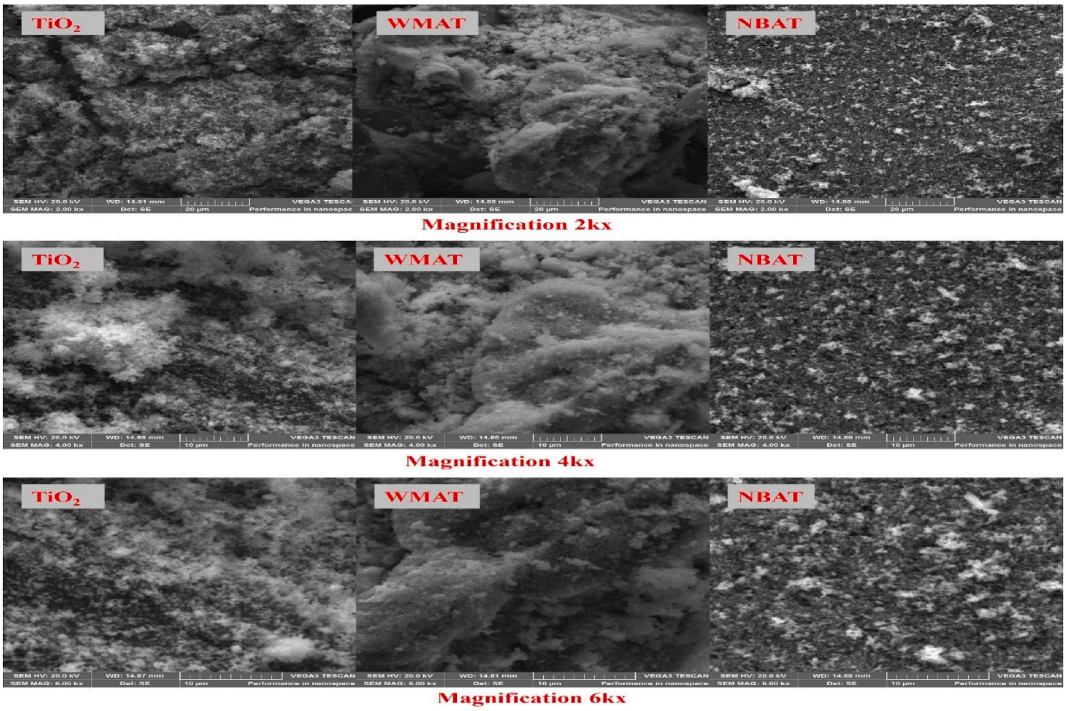

Fig. 7. SEM images of the TiO_2 nanoparticles and synthesized nanocomposites at different scales of magnification (2kx, 4kx, and 6kx).

more suitable. The lack of a capping agent in chemical synthesis was anticipated to cause agglomeration. However, this agglomeration was only observed when the synthesis was carried out using WMRE. Further research is required to explore the agglomerating effect of plant extract capping agents.

3.7. TEM micrographs for the synthesized nanocomposites

The TEM micrographs of TiO_2, WMAT, and NBAT are shown in Fig. 8, including inserts of higher magnification (50 nm). The spherical TiO_2 nanoparticles had an average diameter of 152.62 ± 64.11 nm. Notably, they also had a thin irregular layer attributed to the presence of Al_2O_3 coating [22]. This was confirmed by the observed elemental Al in the TiO_2 nanoparticles, WMAT, and NBAT during EDS elemental analysis (Fig. 5). During commercial synthesis, TiO_2 is treated with an Al_2O_3 layer to enhance photocatalytic activity and stability. Furthermore, surface modification with Ag nanoparticles only occurs in areas without the Al_2O_3 layer [48].

Although the Ag nanoparticles were spherical for both synthesis methods, they differed in size. For instance, chemical synthesis yielded Ag nanoparticles with an average diameter of 14.87 ± 14.61 nm, whereas green synthesis yielded Ag nanoparticles with an average diameter of 7.48 ± 4.06 nm. This pointed to the WMRE efficiency as a reducing and capping agent to form small and highly monodisperse Ag nanoparticles. Similarly, Ndikau et al. [6] established that WMRE-mediated synthesis of Ag nanoparticles results in smaller and more stable nanoparticles compared to chemical synthesis using trisodium citrate.

Even though WMRE has been used by Ndikau et al. [6] to synthesize Ag nanoparticles, their modification on TiO_2 using WMRE has yet to be reported. Ultimately, this work shows that green synthesis of Ag/TiO_2 can effectively replace chemical synthesis. Additionally, green synthesis offers the benefits of meeting the principles of green chemistry while resulting in the synthesis of better nanoparticles [1,29,49]. Focus is therefore aimed more at evaluating the effects of the synthesis conditions and ensuring the reproducibility of green synthesis methods [50].

4. Conclusion

In summary, Ag/TiO_2 nanocomposite was successfully synthesized via an aqueous reduction method using the *Citrullus lanatus rind* extract as the reducing and stabilizing agent. The evaluation of the reaction parameters showed that the synthesis process was most effective at a temperature of 100 °C, a pH of 12, and a reaction time of 45 min. This resulted in the formation of spherical Ag nanoparticles with an average diameter of 7.48 ± 4.06 nm, which were deposited on the surface of the TiO_2 nanoparticles. This uniformity was attributed to the stabilization effects of the C=O functional groups, which were identified using FTIR analysis with an absorption peak at 1649 cm^{-1}. However, the morphological study revealed some agglomeration in this nanocomposite, which was linked to the presence of these functional groups. On the other hand, the chemical synthesis of Ag/TiO_2 yielded spherical Ag nanoparticles with an average diameter of 14.61 ± 14.87 nm modified on the surface of the TiO_2 nanoparticles. Even though both synthesis

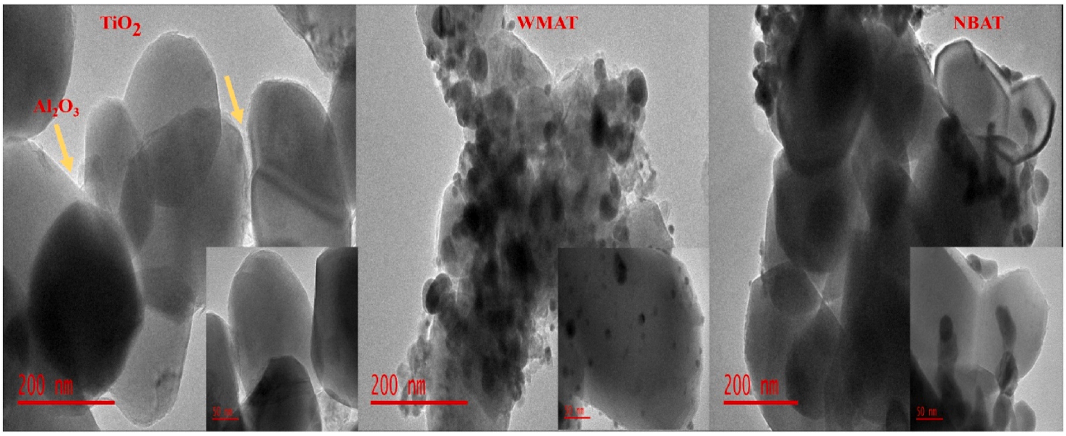

Fig. 8. TEM images of TiO_2, WMAT, and NBAT with inserts of higher magnification (50 nm).

methods yielded visible light activity, indicating improved TiO_2 photocatalytic activity, green synthesis yielded better visible light activity. These results indicate that using *Citrullus lanatus* rind extract to synthesize Ag/TiO_2, an environmentally safe, effective, easy, and cost-effective process, could potentially replace chemical synthesis.

Funding information

This work was partially supported by the United States Environment Protection Agency (EPA), grant number SU839297.

Data availability

Data will be made available on request.

CRediT authorship contribution statement

Marylyn Mugure Gathiru: Writing – original draft, Visualization, Software, Resources, Methodology, Investigation, Formal analysis, Data curation. **Emilly Obuya:** Writing – review & editing, Supervision, Resources, Project administration, Methodology, Funding acquisition, Conceptualization. **Naumih M. Noah:** Writing – review & editing, Supervision, Resources, Project administration, Methodology. **Erick Masika:** Writing – review & editing, Supervision, Methodology.

Declaration of competing interest

The authors declare the following financial interests/personal relationships which may be considered as potential competing interests:Emilly Obuya reports financial support was provided by United States Environmental Protection Agency. If there are other authors, they declare that they have no known competing financial interests or personal relationships that could have appeared to influence the work reported in this paper.

References

[1] A.M. El Shafey, Green synthesis of metal and metal oxide nanoparticles from plant leaf extracts and their applications: a review, Green Process. Synth. 9 (1) (2020) 304–339, https://doi.org/10.1515/gps-2020-0031.
[2] G. Vasyliev, V. Vorobyova, Valorization of food waste to produce eco-friendly means of corrosion protection and 'green' synthesis of nanoparticles, Adv. Mater. Sci. Eng. 2020 (2020), https://doi.org/10.1155/2020/6615118.
[3] S. Dubey, H. Rajput, K. Batta, "Utilization of watermelon rind (Citrullus lanatus) in various food preparations, A Review 11 (41) (2021) 77–82, https://doi.org/10.37273/chesci.cs205205361.
[4] A.H. Hashem, et al., Watermelon rind mediated biosynthesis of bimetallic selenium-silver nanoparticles: characterization, antimicrobial and anticancer activities, Plants 12 (18) (2023) 1–17, https://doi.org/10.3390/plants12183288.
[5] M. Mushtaq, B. Sultana, H.N. Bhatti, M. Asghar, RSM based optimized enzyme-assisted extraction of antioxidant phenolics from underutilized watermelon (Citrullus lanatus Thunb.) rind, J. Food Sci. Technol. 52 (8) (2015) 5048–5056, https://doi.org/10.1007/s13197-014-1562-9.
[6] M. Ndikau, N.M. Noah, D.M. Andala, E. Masika, Green synthesis and characterization of silver nanoparticles using Citrullus lanatus fruit rind extract, Int. J. Anal. Chem. 2017 (2017), https://doi.org/10.1155/2017/8108504.
[7] J. Sackey, et al., Molecular dynamics and bio-synthesis of phoenix dactylifera mediated Mn3O4 nanoparticles: electrochemical application, J. Alloys Compd. 854 (2021) 156987, https://doi.org/10.1016/j.jallcom.2020.156987.
[8] M. Fang, X. Tan, Z. Liu, B. Hu, X. Wang, Recent progress on metal-enhanced photocatalysis: a review on the mechanism, Research 2021 (2021), https://doi.org/10.34133/2021/9794329.
[9] O.K. Dalrymple, D.Y. Goswami, Mechanistic Modeling of Photocatalytic Water Disinfection, 2017, pp. 273–315, https://doi.org/10.1007/978-3-662-53496-0_13.

[10] S. Gunti, Enhanced Visible Light Photocatalytic Remediation of Organics in Water Using Zinc Oxide and Titanium Oxide Nanostructures, June, 2017 [Online]. Available:.
[11] D. Hariharan, et al., Enhanced photocatalysis and anticancer activity of green hydrothermal synthesized Ag@TiO2 nanoparticles, J. Photochem. Photobiol. B Biol. 202 (September 2019) (2020) 111636, https://doi.org/10.1016/j.jphotobiol.2019.111636.
[12] D.M. Tobaldi, L. Lajaunie, M.P. Seabra, R. Arenal, "TiO 2 Surface Hybridisation with Noble Metals (Ag and Cu X O) for Solar De-NO X and VOC Removal,", vol. 1, 2020, pp. 1–26, https://doi.org/10.26434/chemrxiv.12198309.v1, x.
[13] W.J. Chen, K.C. Hsu, T.H. Fang, C.I. Lee, T.H. Chen, T.H. Hsieh, Structural, optical characterization and photocatalytic behavior of Ag/TiO2 nanofibers, Dig. J. Nanomater. Biostruct. 16 (4) (2021) 1227–1234.
[14] A. Di Bartolomeo, Graphene Schottky diodes: an experimental review of the rectifying graphene/semiconductor heterojunction, Phys. Rep. 606 (2016) 1–58, https://doi.org/10.1016/j.physrep.2015.10.003. June 2015.
[15] P. Jegadeeswaran, P. Rajiv, P. Vanathi, S. Rajeshwari, R. Venckatesh, A novel green technology: synthesis and characterization of Ag/TiO2 nanocomposites using Padina tetrastromatica (seaweed) extract, Mater. Lett. 166 (2016) 137–139, https://doi.org/10.1016/j.matlet.2015.12.058.
[16] J. Torres-Limiñana, A.A. Feregrino-Pérez, M. Vega-González, L. Escobar-Alarcón, J.A. Cervantes-Chávez, K. Esquivel, Green synthesis via Eucalyptus globulus L. Extract of Ag-TiO2 catalyst: antimicrobial activity evaluation toward water disinfection process, Nanomaterials 12 (11) (2022), https://doi.org/10.3390/nano12111944.
[17] F.O. Purnomo, S.S. Ningrum, S.N. Kautsari, Synthesis and characterization of Ag/TiO2 nanoparticles using Mirabilis jalapa plant extract, J. Kim. Val. 7 (1) (2021) 22–27, https://doi.org/10.15408/jkv.v7i1.18875.
[18] M. Skiba, V. Vorobyova, K. Sorochkina, Bio-green and classical stabilize agents of nanoparticles in silver-doped titanium dioxide: the influence on antioxidant, photocatalytic, and bactericidal activities, Plasmonics 17 (5) (Oct. 2022) 2221–2234, https://doi.org/10.1007/s11468-022-01706-8.
[19] M.I. Skiba, V.I. Vorobyova, I.V. Kosogina, Preparation of silver nanoparticles in a plasma-liquid system in the presence of PVA: antimicrobial, catalytic, and sensing properties, J. Chem. 2020 (2020), https://doi.org/10.1155/2020/5380950.
[20] P.S. Yerragopu, S. Hiregoudar, U. Nidoni, K.T. Ramappa, A.G. Sreenivas, S.R. Doddagoudar, Chemical synthesis of silver nanoparticles using tri-sodium citrate, stability study and their characterization, Int. Res. J. Pure Appl. Chem. 21 (3) (2020) 37–50, https://doi.org/10.9734/irjpac/2020/v21i330159.
[21] M. Skiba, V. Vorobyova, Green synthesis and characterization of silver nanoparticles using Prunus persica L. (peach pomace) with natural deep eutectic solvent and plasma-liquid process, Chem. Pap. 76 (9) (Sep. 2022) 5789–5806, https://doi.org/10.1007/s11696-022-02274-1.
[22] N. Niño-Martínez, G.A. Martínez-Castañón, A. Aragón-Piña, F. Martínez-Gutierrez, J.R. Martínez-Mendoza, F. Ruiz, Silver nanoparticles synthesized on titanium dioxide fine particles, in: Tech. Proc. 2008 NSTI Nanotechnol. Conf. Trade Show, NSTI-Nanotech, Nanotechnol, vol. 1, 2008, pp. 737–740, https://doi.org/10.1088/0957-4484/19/6/065711, 2008.
[23] Y.S. Liu, Y.C. Chang, H.H. Chen, Silver nanoparticle biosynthesis by using phenolic acids in rice husk extract as reducing agents and dispersants, J. Food Drug Anal. 26 (2) (2018) 649–656, https://doi.org/10.1016/j.jfda.2017.07.005.
[24] M. Ismail, S. Gul, M.I. Khan, M.A. Khan, A.M. Asiri, S.B. Khan, Medicago polymorpha-mediated antibacterial silver nanoparticles in the reduction of methyl orange, Green Process. Synth. 8 (1) (2019) 118–127, https://doi.org/10.1515/gps-2018-0030.
[25] S.N.H.M. Azmin, Z.A. Manan, S.R.W. Alwi, L.S. Chua, A.A. Mustaffa, N.A. Yunus, Herbal processing and extraction technologies, Separ. Purif. Rev. 45 (4) (2016) 305–320, https://doi.org/10.1080/15422119.2016.1145395.
[26] L.H. Ho, N.F. Ramli, T.C. Tan, N. Muhamad, M.N. Haron, Effect of extraction solvents and drying conditions on total phenolic content and antioxidant properties of watermelon rind powder, Sains Malays. 47 (1) (2018) 99–107, https://doi.org/10.17576/jsm-2018-4701-12.
[27] X. Wang, Y. Cao, Characterizations of absorption, scattering, and transmission of typical nanoparticles and their suspensions, J. Ind. Eng. Chem. 82 (2020) 324–332, https://doi.org/10.1016/j.jiec.2019.10.030.
[28] C.S. Seney, B.M. Gutzman, R.H. Goddard, Correlation of size and surface-enhanced Raman scattering activity of optical and spectroscopic properties for silver nanoparticles, J. Phys. Chem. C 113 (1) (2009) 74–80, https://doi.org/10.1021/jp805698e.
[29] N. Kobese, Synthesis of Silver Doped Titanium Dioxide Nanocomposites Using Tea Extract from Aspalathus Linearis and Evaluation of Their Antibacterial Effects, By Nokubonga Kobese," no. September, 2018 [Online]. Available, http://hdl.handle.net/11394/6779.
[30] M. Amin, F. Anwar, M.R.S.A. Janjua, M.A. Iqbal, U. Rashid, Green synthesis of silver nanoparticles through reduction with Solanum xanthocarpum L. berry extract: characterization, antimicrobial and urease inhibitory activities against Helicobacter pylori, Int. J. Mol. Sci. 13 (8) (2012) 9923–9941, https://doi.org/10.3390/ijms13089923.
[31] D.A. Méndez, M.J. Fabra, L. Gómez-Mascaraque, A. López-Rubio, A. Martinez-Abad, Modelling the extraction of pectin towards the valorisation of watermelon rind waste, Foods 10 (4) (2021), https://doi.org/10.3390/foods10040738.
[32] M.J. Jensen, P.A. Fuierer, Low-temperature preparation of nanocrystalline anatase films through a sol-gel route, J. Sol. Gel Sci. Technol. 39 (3) (2006) 229–233, https://doi.org/10.1007/s10971-006-7837-5.
[33] E.H. Alsharaeh, et al., Sol-gel-assisted microwave-derived synthesis of anatase Ag/Tio2/Go nanohybrids toward efficient visible light phenol degradation, Catalysts 7 (5) (2017), https://doi.org/10.3390/catal7050133.
[34] T. Wei, et al., A functional applied material on recognition of metal ion zinc based on the double azine compound, Tetrahedron 73 (20) (2017) 2938–2942, https://doi.org/10.1016/j.tet.2017.04.001.
[35] S. Yan, C. Chen, F. Zhang, S.A. Mahyoub, Z. Cheng, High-density Ag nanosheets for selective electrochemical CO2 reduction to CO, Nanotechnology 32 (16) (2021), https://doi.org/10.1088/1361-6528/abd6af.
[36] Z. Fayyaz, M.A. Farrukh, A. Ul-Hamid, K.K. Chong, Elucidating the structural, catalytic, and antibacterial traits of Ficus carica and Azadirachta indica leaf extract-mediated synthesis of the Ag/CuO/rGO nanocomposite, Microsc. Res. Tech. 87 (5) (2024) 957–976, https://doi.org/10.1002/jemt.24487.
[37] K. Mallikarjuna, et al., Green synthesis of silver nanoparticles using Ocimum leaf extract and their characterization, Dig. J. Nanomater. Biostruct. 6 (1) (2011) 181–186 [Online]. Available: https://api.semanticscholar.org/CorpusID:29059333.
[38] T. Siddiqui, M.K. Zia, M. Muaz, H. Ahsan, F.H. Khan, Synthesis and characterization of silver nanoparticles (AgNPs) using chemico-physical methods, IJCA (Indonesian J. Chem. Anal. 6 (2) (2023) 124–132, https://doi.org/10.20885/ijca.vol6.iss2.art4.
[39] R. Javed, M. Zia, S. Naz, S.O. Aisida, N. ul Ain, Q. Ao, Role of capping agents in the application of nanoparticles in biomedicine and environmental remediation: recent trends and future prospects, J. Nanobiotechnol. 18 (1) (2020) 1–15, https://doi.org/10.1186/s12951-020-00704-4.
[40] B.S. A, et al., GC-MS and FTIR analysis of aqueous extract of citrillus lanatus (water Melon) rind, Sch. Int. J. Biochem. 5 (4) (2022) 57–66, https://doi.org/10.36348/sijb.2022.v05i04.001.
[41] L. Poto, et al., Cross calibration between XRF and ICP-MS for high spatial resolution analysis of ombrotrophic peat cores for palaeoclimatic studies, Anal. Bioanal. Chem. 407 (2) (2015) 379–385, https://doi.org/10.1007/s00216-014-8289-3.
[42] M. Ali, "Determining and Quantifying Chemically Produced Stresses in (Atoms of) Electronic and Crystalline Materials,", 2024, https://doi.org/10.13140/RG.2.2.23849.40808. March.
[43] M.H. Habibi, M. Nasr-Esfahani, Silver doped TiO 2 nanostructure composite photocatalyst film synthesized by sol-gel spin and dip coating technique on glass, Int. J. Photoenergy 2008 (2008), https://doi.org/10.1155/2008/628713.
[44] A.A. Mosquera, J.M. Albella, V. Navarro, D. Bhattacharyya, J.L. Endrino, Effect of silver on the phase transition and wettability of titanium oxide films, Sci. Rep. 6 (July) (2016) 1–14, https://doi.org/10.1038/srep32171.
[45] S. Rabhi, et al., Tuning the photocatalytic activity of TiO2 by Ag loading: experimental and modelling studies for the degradation of amlodipine besylate drug, Ceram. Int. 47 (15) (2021) 21509–21521, https://doi.org/10.1016/j.ceramint.2021.04.162.
[46] A.R. Zanatta, A fast-reliable methodology to estimate the concentration of rutile or anatase phases of TiO2, AIP Adv. 7 (7) (2017) 1–7, https://doi.org/10.1063/1.4992130.
[47] M. Aminuzzaman, L.P. Ying, W.S. Goh, A. Watanabe, Green synthesis of zinc oxide nanoparticles using aqueous extract of Garcinia mangostana fruit pericarp and their photocatalytic activity, Bull. Mater. Sci. 41 (2) (2018), https://doi.org/10.1007/s12034-018-1568-4.

[48] N. Veronovski, TiO2 applications as a function of controlled surface treatment, Titan. Dioxide - Mater. a Sustain. Environ. (2018), https://doi.org/10.5772/intechopen.72945.
[49] M. Nasrullah, et al., Green and chemical syntheses of CdO NPs: a comparative study for yield attributes, biological characteristics, and toxicity concerns, ACS Omega 5 (11) (2020) 5739–5747, https://doi.org/10.1021/acsomega.9b03769.
[50] J. Narang, K. Rani, I. Sonia, C. Singhal, Green versus chemical synthesis of gold and silver nanoparticles, J. Bionanoscience 10 (5) (2016) 341–347, https://doi.org/10.1166/jbns.2016.1389.